

New Gain Parameterization for Fast Semiconductor Optical Amplifier Model

Pascal Lemieux^a, Walid Mathlouthi^a, Massimiliano Salsi^b, Leslie A. Rusch^a, Armando Vannucci^b and Alberto Bononi^b

^aCentre d'Optique, Photonique et Lasers, Université Laval, Québec, Canada;

^bDipartimento di Ingegneria dell'Informazione, Università degli Studi di Parma, Parma, Italy

ABSTRACT

Numerical simulations of semiconductor optical amplifiers (SOA) often are time consuming. Making simplifying assumptions, we obtain a fast model based on the *reservoir*, representing the total number of useful carriers. In this paper, we explain how this model is developed and how the gain is parameterized. We demonstrate that the scattering losses, dropped in the derivation of the reservoir model, can be re-introduced by applying a simple transformation to the gain coefficient. In this way, the accuracy of the model is greatly increased, but its level of complexity remains low.

Keywords: Semiconductor optical amplifier (SOA), numerical model, gain parameterization, optical communications

1. INTRODUCTION

Semiconductor optical amplifiers (SOA) are considered important components for the next generation of optical networks. They can be used in a wide variety of applications, including optical switching and wavelength conversion using or cross-gain modulation^{1,2} (XGM). Other applications include signal reshaping and noise cleaning of on-off keying (OOK) signals.³ The latter application has been demonstrated for optical communication systems using multiplexed spectrum-sliced sources (SSWDM) at bit rates under 10 Gb/s which are applicable to metropolitan area networks.⁴

Keeping in mind our objective of evaluating the performance of systems at relatively low bit rates, it is reasonable to neglect the effects of ultrafast phenomena in the numerical SOA models. The intraband phenomena such as spectral hole burning (SHB) and carrier heating (CH) operating in the femtosecond range⁵ are neglected, and the model accounts only for the gain dynamics of the SOA.

The available numerical SOA models can be divided in two categories: 1) space-resolved, numerically intensive models and 2) analytical, simplified models developed to facilitate performance analysis. In this paper, we discuss a detailed space-resolved model, presented by Connelly,⁶ taking into account facet reflectivity as well as forward and backward propagating amplified spontaneous emission (ASE). This model is based on a set of coupled partial differential equations (PDE) that must be solved simultaneously. To carry out extensive Monte-Carlo simulations for statistical signal analysis and bit-error rate (BER) estimation, accurate space-resolved models are ruled out because of the prohibitively long simulation times.

To enable such simulations, we discuss some simplifying assumptions that can be made to reduce the complexity of the space-resolved model. This model is based on a quantity called the reservoir, which is the total number of carriers in the SOA. The approximations used in the derivation ultimately lead to a single ordinary differential equation (ODE). Although the simplified *reservoir* model obtained with these simplifications gives a coarser fit with experimental data than the space-resolved model, the execution time required for numerical simulations is greatly reduced. The improvement in calculation time is significant, allowing for extensive Monte-Carlo simulations of the BER. More than just execution speed, the reservoir model also has another interesting feature.

Further author information: (Send correspondence to Leslie Ann Rusch)
L.A.R.: E-mail: rusch@gel.ulaval.ca, Telephone: 1 (418) 656-2906

It is amenable to a block diagram representation, which could lead to a mathematically elegant stochastic performance analysis similar to the one done by Saleh *et al.*⁷ on single-channel saturated SOAs.

The reservoir model does not however contain a description of the SOA gain based on its physical properties (temperature, material, gap energy, etc.). Here, we propose a way to parameterize the reservoir model using the gain description based on semiconductor physics. The impact of the scattering losses is discussed and we show that it is possible to include these losses either 1) directly in the gain coefficient description or 2) by adding lumped losses. The numerical simulation results obtained with these techniques are then compared with experimental data.

2. SPACE-RESOLVED MODEL

In this section, we choose a wideband numerical SOA model proposed by Connelly⁶ as a starting point to develop a faster model. The detailed space-resolved model is based on the numerical solution of a set of coupled PDEs. These equations describe 1) the temporal and spatial variations of carrier density $n(z, t)$ and 2) the photon flux for both forward (+) and backward (-) propagating spectral components of signal and ASE. It is important to note that the carrier density $n(z, t)$ in this model is already averaged over the cross-section of the amplifier, meaning that the our space-resolved model does not consider variation of the carrier density on the x and y axes. Furthermore, the space-resolved model does not consider the electric fields of the signals. It only considers the respective signal's power and thus neglects the phase from the start.

2.1. Rate Equation

The first differential equation describing the behavior of the SOA is the *rate equation*, which is common to all signals and ASE components. According to Connelly,⁶ the rate equation can be expressed as

$$\frac{\partial n(z, t)}{\partial t} = \frac{I_{bias}}{qWdL} - R(n) - \frac{\Gamma}{A} \sum_{k=1}^{N_{sig}} g_{mat}(\lambda_k, n) [Q_k^+ + Q_k^-] - \sum_{j=1}^{N_{ASE}} f_{ASE}(\lambda_j, n) \quad (1)$$

where Q_k is the number of photons at wavelength λ_k , I_{bias} the bias current applied on the gain region, q the electron charge, L the length, $A = Wd$ the rectangular cross-section of the active region and Γ the confinement factor. The index k is used for the wavelengths of signals while j is used for ASE wavelengths. The gain coefficient $g_{mat}(\lambda_k, n)$ is described in Section 4.1. The term $R(n)$ represents the spontaneous recombinations and is a polynomial function of the carrier density,⁶ that can be approximated as n/τ . The depletion of the carriers induced by the ASE, represented by $f_{ASE}(\lambda, n)$, is given by

$$f_{ASE}(\lambda_j, n(z)) = \frac{2\Gamma}{A} g_{mat}(\lambda_j, n(z)) [Q_j^+(z) + Q_j^-(z)] \quad (2)$$

The factor of 2 in (2) accounts for the two possible orthogonal polarisations of the ASE components. The rate equation must be solved for each one of the N_z slices along the z axis of the SOA (see Figure 1). A global solution is achieved when all slices are in equilibrium, meaning that the photon fluxes coming in and going out of each slice lead to a stable carrier density inside each and every slice. The number of photons used in (1) is related to the optical power by

$$Q_k^\pm = |E_k^\pm|^2 \frac{\lambda_k}{hc} = P_k^\pm \frac{\lambda_k}{hc} \quad (3)$$

where h is Planck's constant. The optical frequency ν is related to the wavelength by $\lambda = c/\nu$ where c is the speed of light. Note that using (1), we neglect the pulsation of the carrier density due to beating among spectral components that is responsible for FWM and cross-phase modulation (XPM) in SOAs.¹

2.2. Propagation Equation

The second part of the set of coupled PDEs in the space-resolved model is formed by the propagation equations, representing the evolution of the photo fluxes along the amplifier's propagation axis z . The propagation equation of each signal component must be solved simultaneously with the rate equation presented in Section 2.1. For each of the N_{sig} signals entering the SOA, the number of photons evolves along the propagation according to

$$\frac{\partial Q_k^\pm(z)}{\partial z} = \pm \left[\Gamma g_{mat}(\lambda_k, z) - \alpha(n) \right] Q_k^\pm(z) . \quad (4)$$

The term $\alpha(n(z))$ represents the scattering losses and is described in Section 4.3. The propagation equation for ASE components is different, since new photons are generated by spontaneous electron-hole recombinations at every SOA slice. Thus, the propagation equation for the ASE components is

$$\frac{\partial Q_j^\pm(z)}{\partial z} = \pm \left[\Gamma g_{mat}(\lambda_j, z) - \alpha(n) \right] Q_j^\pm(z) + R_{sp}(\lambda_j, z) \quad (5)$$

where the term $R_{sp}(\lambda_j, z)$ was added in (5) to represent the spontaneous emission at λ_j . The steady-state solution is obtained by adjusting the carrier density on each section of the SOA, using the algorithm presented by Connelly.⁶ A representation of the steady-state algorithm is shown in the upper part of Figure 1. A time-varying numerical solution to the coupled PDEs is obtained based on the assumption that the carrier density $n(z, t)$ remains constant within a time step, as explained by Mathlouthi *et al.*⁸

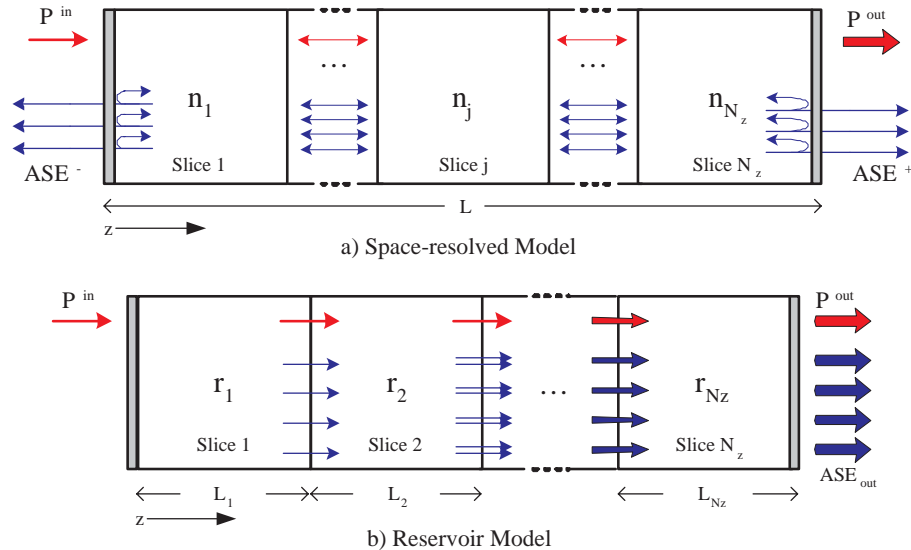


Figure 1. Graphical representation of the numerical algorithms used for the space-resolved and reservoir models

3. RESERVOIR MODEL

3.1. Derivation of the Reservoir Model

We now present the derivation of a fast and efficient SOA model called the *reservoir* model. In this derivation, we assume a travelling-wave amplifier (zero facet reflectivity) meaning that all spectral components travel in the same direction. We begin by rewriting the rate equation of the space-resolved model

$$\frac{\partial n(z, t)}{\partial t} = \frac{I_{bias}}{qV} - R(n) - \frac{\Gamma}{A} \sum_{k=1}^{N_{sig}} g_{mat}(\lambda_k, n) Q_k(z, t) - \frac{4\Gamma}{A} \sum_{j=1}^{N_{ASE}} g_{mat}(\lambda_j, n) Q_j(z, t) \quad (6)$$

where the forward ASE photon flux is assumed to be twice that of (2) to keep the same level of saturation caused by the ASE power inside the amplifier. It is a simplified way to consider the effect of propagation on the ASE components. The difference in the modeling of the propagation in both models is represented graphically in Figure 1. The upper part of this figure shows the space-resolved model and the lower part the reservoir model, where all photon fluxes are oriented from $z = 0$ to $z = L$. To increase the calculation speed, we choose to remove the spatial resolution on the carrier density $n(z, t)$ by integrating the rate equation. The space resolution can be reintroduced if necessary under certain assumptions.⁸ Note that the reservoir can describe both forward and reverse propagating signals, but only ASE in one direction. We start by defining a new variable

$$r(t) \equiv A \int_0^L n(z, t) dz \quad (7)$$

called the *reservoir* and representing the total number of carriers in the amplifier. By integrating (6) over the amplifier's length and multiplying by the cross-section A , we obtain

$$\frac{dr(t)}{dt} = \frac{I_{bias}}{q} - \frac{r(t)}{\tau} - \sum_{k=1}^{N_{sig}} \int_0^L \Gamma g_{mat}(\lambda_k, n(z)) Q_k(z, t) dz - 4 \sum_{j=1}^{N_{ASE}} \int_0^L \Gamma g_{mat}(\lambda_j, n(z)) Q_j(z, t) dz . \quad (8)$$

The ASE contribution, the last term on the right hand side of (8), is neglected for the time being. The first summation term on the right hand side can be expressed more elegantly by integrating the propagation equation, considering again photons propagating in one direction. In these conditions, the photon number Q_k is replaced by its equivalent power P_k using (3) and the integration of (4) yields

$$\int_0^L \Gamma g_{mat}(\lambda_k, n) Q_k(z, t) dz = [P_k^{out}(t) - P_k^{in}(t)] + \int_0^L P_k(z, t) \alpha(n) dz \quad (9)$$

where the optical power at the input of the amplifier ($z = 0$) is given by $P_k^{in}(t)$ and the power at the output ($z = L$) is given by $P_k^{out}(t)$. As suggested by Agrawal,⁹ we assume that the gain is typically much greater than the losses in an amplifier and that the loss term $\alpha(n)$ can be neglected in the propagation equation. The approximation involved in dropping this term will be discussed in Section 4.3. The reservoir equation (without the ASE and scattering losses contributions) then becomes

$$\frac{dr(t)}{dt} = \frac{I_{bias}}{q} - \frac{r(t)}{\tau} - \sum_{k=1}^{N_{sig}} \frac{\lambda_k}{hc} [P_k^{out}(t) - P_k^{in}(t)] . \quad (10)$$

In order to facilitate an analytic integration of (9), we assume that the gain coefficient can be approximated by $g_{mat} \cong \sigma_k(n - \eta_{0,k})$ and the global gain $G \equiv P_{out}/P_{in}$ is then expressed by

$$G(\lambda_k, n) \cong \exp \left(\Gamma \int_0^L \sigma_k(n - \eta_{0,k}) dz \right) \quad (11)$$

$$\cong \exp \left(\Gamma \frac{\sigma_k}{A} (r - AL \eta_{0,k}) \right) \quad (12)$$

where $AL \eta_{0,k} \equiv r_{0,k}$ represents the reservoir at transparency at wavelength λ_k . By definition of the reservoir at transparency, $g_{mat}(\lambda_k, \eta_{0,k}) = 0$. The term σ_k/A represents the slope of the gain coefficient as a function of the reservoir r . Using this approximation of the gain coefficient and neglecting ASE, the reservoir equation can be expressed as

$$\frac{dr(t)}{dt} = \frac{I_{bias}}{q} - \frac{r(t)}{\tau} - \sum_{k=1}^{N_{sig}} \frac{\lambda_k}{hc} P_k^{in}(t) \left[\exp \left(\Gamma \frac{\sigma_k}{A} (r - r_{0,k}) \right) - 1 \right] \quad (13)$$

Based on the ordinary differential equation (13) only, the reservoir model allows for a much faster numerical solution than the space-resolved model. The propagation equations have been integrated into the rate equation and the output power is given by

$$P_k^{out}(t) = P_k^{in}(t) \exp \left[\Gamma \frac{\sigma_k}{A} (r(t) - r_{0,k}) \right] \quad (14)$$

The linearized gain coefficients σ_k and $\eta_{0,k}$ can be modified to take into account the scattering losses neglected in (9). The procedure is explained in Section 4.2 and the numerical results are presented in Sections 5.1 to 5.3. In the derivation of the reservoir model, the ASE term in (8) was put aside. Taking into account the ASE contribution (specific to the reservoir ODE) will lead to the complete reservoir dynamic equation⁸

$$\frac{dr(t)}{dt} = \frac{I_{bias}}{q} - \frac{r}{\tau} - \sum_{k=1}^{N_{sig}} \frac{\lambda_k}{hc} [P_k^{out}(t) - P_k^{in}(t)] - \sum_{j=1}^{N_{ASE}} \eta_{sp,j} [G_j(r) - 1 - \ln(G_j(r))] . \quad (15)$$

The reservoir model derivation presented in this section reduces the space-resolved model to a punctual model, i.e. without spacial resolution. However, it is possible trade complexity for precision by dividing the amplifier in a cascade of smaller amplifiers. The original SOA of length L is divided in N_z slices and each of these slices then has its own reservoir. The output of one slice then becomes the input of the next one, still assuming that all spectral components travel in the same direction. This cascade of smaller SOA is presented in Figure 1.

3.2. Experimental Validation of the Model

In this section, we explain how we can verify that our reservoir model captures the important signal performance characteristics provided by the space-resolved model and matches measurements of our physical SOA. To do so, we define three figures of merit that cover both the static and dynamic regimes. These figures of merit are

- the gain saturation curve $G(P_{in})$ at $\lambda = 1560$ nm where the gain is maximum (static),
- the gain spectrum $G(\lambda)$ at a fixed input power $P_{in} = -27$ dBm where the SOA is not saturated (static),
- the shape $P(t)$ of an amplified optical pulse at the output of the SOA (dynamic).

The numerical results for the reservoir model for each figure were compared with the corresponding experimental data obtained with our commercial Optospeed SOA (model 1550MRI X1500) biased at 500 mA. To measure the gain saturation and the gain spectrum, we used a tunable CW laser Agilent (model 8164A) at the input of the SOA and measured the output power with a calibrated Ando OSA (model AQ6317B). The gain was calculated according to the techniques described by Derickson *et al.*¹⁰

The optically amplified pulse shape, or the response of the SOA to a square wave, was obtained using the same tunable laser at 1560 nm. The light source was modulated by a pseudo-random sequence of length $2^7 - 1$ at 1 Gb/s using a Mach-Zender modulator. The average power at the input was fixed at -18 dBm with an extinction ratio around 10 dB. No optical filter was used before photo-detection to include the effects of ASE. The power of the amplified pulse in time domain was detected by an Agilent photo-receiver (model 11982A) and acquired using an Agilent sampling oscilloscope (model 86100A). The experimental procedures are described by Mathlouthi *et al.*⁸ in greater details.

4. GAIN PARAMETERIZATION

In the previous section, the gain coefficient $g_{mat}(\lambda, n)$ was supposed linear for each wavelength. However, we did not explain how the parameters $\sigma(\lambda)$ and $\eta_0(\lambda)$ could be obtained. We present first a technique discussed by Connelly⁶ to obtain the value of $g_{mat}(\lambda, n)$. Then we explain how to extract the parameters of the linear fit $\sigma(\lambda)$ and $\eta_0(\lambda)$ and how to use them within the reservoir model.

4.1. Gain Coefficient

From the basic properties of the active region's material and the physics of semiconductors, an expression for the gain coefficient can be obtained. It is based on the probability of a photon of wavelength λ_k stimulating an electron-hole recombination in the active region. It is thus based on the probability of finding an electron in the conduction band $f_c(\lambda)$ and a hole on the valence band $f_v(\lambda)$. The model also considers the impact of the temperature and the injection current on the Fermi levels, and the gap energy between the two bands is corrected using the relation

$$E_g(n) = E_{g0} - qK_g n^{1/3} \quad (16)$$

where E_{g0} is the gap energy at zero injected carriers, and K_g is the bandgap shrinkage coefficient having a value of $0.1 \cdot 10^{-10}$ eV·m for our Optospeed SOA. With this relation, it is possible to obtain the following expression⁶

$$g_{mat}(\lambda, n) = \frac{\lambda^2}{4\sqrt{2}\pi^{3/2}n_1^2\tau} \left(\frac{2m_e m_{hh}}{h(m_e + m_{hh})} \right)^{3/2} \left(\frac{c}{\lambda} - \frac{E_g(n)}{h} \right)^{1/2} [f_c(\lambda) - f_v(\lambda)]. \quad (17)$$

where n_1 is the refractive index of the active region, τ the radiative lifetime of the carriers, ν the optical frequency, h the Planck's constant, m_e the effective mass of an electron and m_{hh} the effective mass of a heavy hole. This gain coefficient $g_{mat}(\lambda, n)$ can be decomposed in two different parts: a pure gain coefficient g'_{mat} and an absorption coefficient g''_{mat} related to the gain coefficient by $g_{mat} = g'_{mat} - g''_{mat}$. The pure gain plays an important role in the ASE description of the reservoir model.⁸ The coefficient g'_{mat} can also be assumed linear, but it has a reservoir at transparency r_1 slightly different from that of the gain coefficient g_{mat} .

4.2. Linearization of the gain coefficient

The gain coefficient $g_{mat}(\lambda, n)$ obtained with (17) and shown in Figure 2 is non-linear when considering n from 0 to ∞ , which contradicts the basic reservoir hypotheses. To respect the initial assumptions of the reservoir model, the gain coefficient must be linear at each wavelength.

The space-resolved model is used to determine the range of achievable values of n over which the gain coefficient is linearized. The limiting values n_{min} and n_{max} are obtained by seeking the minimum or maximum of the carrier density distribution $n(z, t)$ obtained with two optical input powers of 0 dBm and -40 dBm respectively. The gain coefficient is then linearized between n_{min} and n_{max} . In figure 3, we demonstrate that the gain can be approximated by a straight line with a small error, on a span much larger than the region limited by n_{min} and n_{max} . The slope of the gain coefficient as a function of n at wavelength λ_k is called $\sigma(\lambda)$. The carrier density at transparency (when $g_{mat} = 0$) is given by $\eta_0(\lambda)$.

4.3. The Scattering Losses Revisited

The numerical simulation results obtained with the space-resolved model are in good agreement with experimental data as was previously demonstrated.^{6,8} Thus, we assume that our space-resolved model is adequately parameterized and that it describes well the behavior of our commercial Optospeed SOA.

However, employing the description of the gain coefficient from the space-resolved model with the reservoir model does not give equally good results. The gain is largely overestimated, especially for small optical input powers. The loss term $\alpha(n)$ dropped in the derivation of the reservoir model is mainly responsible for this disagreement. Keeping the same gain coefficient while neglecting the losses has the obvious effect of overestimating the gain $G(\lambda, n)$.

To properly describe the gain (both static and dynamic) of the SOA, we study two different methods. The first one subtracts the $\alpha(n)$ term from the gain before any linear assumption. The second method uses the gain $g_{mat}(\lambda, n)$ with the same parameterization, but introduces discrete propagation losses between each section (slice) of the amplifier. Both methods reduce the gain, but their effect on the gain spectrum is quite different.

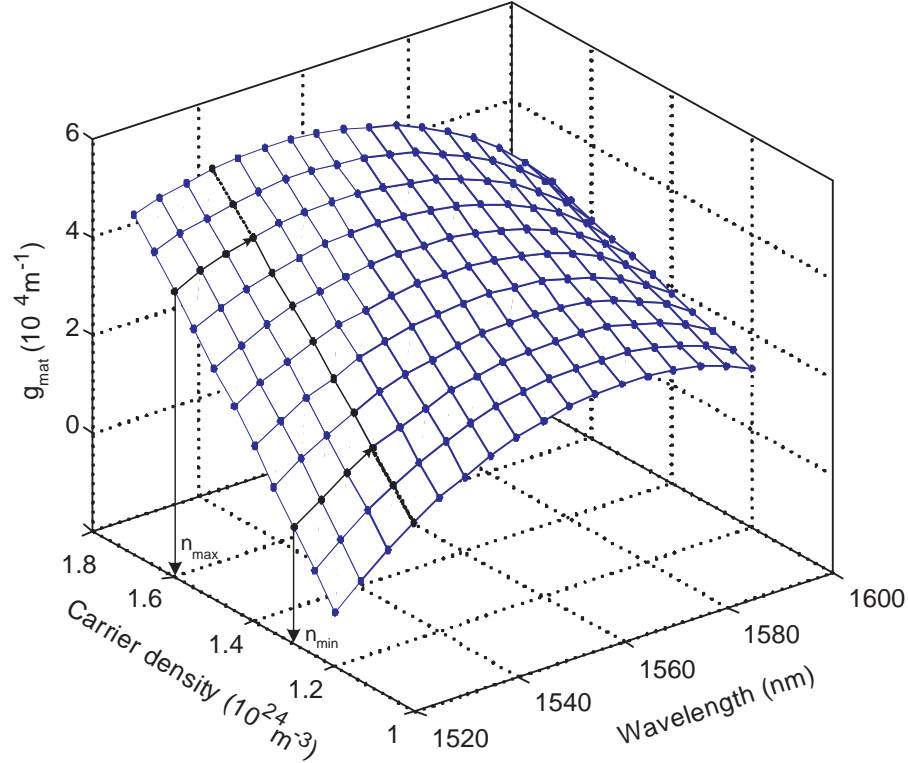


Figure 2. Non-linear gain coefficient $g_{mat}(\lambda, n)$

4.3.1. Method 1: Adjusting the Gain Coefficient

The first method proposed to consider the losses $\alpha(n)$, without adding terms to the reservoir ODE in (15), is to subtract the carrier-dependent loss term from the gain coefficient g_{mat} using the following transformation:

$$g_{res}(\lambda, n) = g_{mat}(\lambda, n) - \frac{\alpha(n)}{\Gamma}. \quad (18)$$

According to previous investigations,^{6,8} the scattering losses can be adequately modeled using a linear relation with the carrier density

$$\alpha(n) \cong K_0 + \Gamma K_1 n. \quad (19)$$

By operating on $g_{mat}(\lambda, n)$ with (18), we reduce the gain coefficient and thus overall gain $G(\lambda, n)$ of the amplifier. The new gain coefficient, called $g_{res}(\lambda, n)$, is also linearized and its slope $a(\lambda)$ and carrier density at transparency $n_0(\lambda)$ are obtained according to the method described in Section 4.2. We then use the parameters a_k and $n_{0,k}$ instead of σ_k and $\eta_{0,k}$ to numerically solve (15).

The transformation of the gain has an important physical signification. It can be interpreted as a mathematical method to reintroduce the scattered carriers back in the active region of the amplifier. By doing so, we reduce the gain observed by the spectral components (signals and ASE) and we overestimate the value of the reservoir. An equivalent reservoir equation, containing an additional term in $\alpha(n)$ can be derived using the procedure presented in Section 3.1. The results obtained with this technique applied to vertically-clamped SOAs are discussed by Salsi *et al.*¹¹

4.3.2. Method 2: Adding Lumped Losses

Another technique to reintroduce in an efficient way the scattering losses dropped from the propagation equations (4) and (5) is to add discretely spaced losses along the propagation axis. At the end of every section (slice) of the

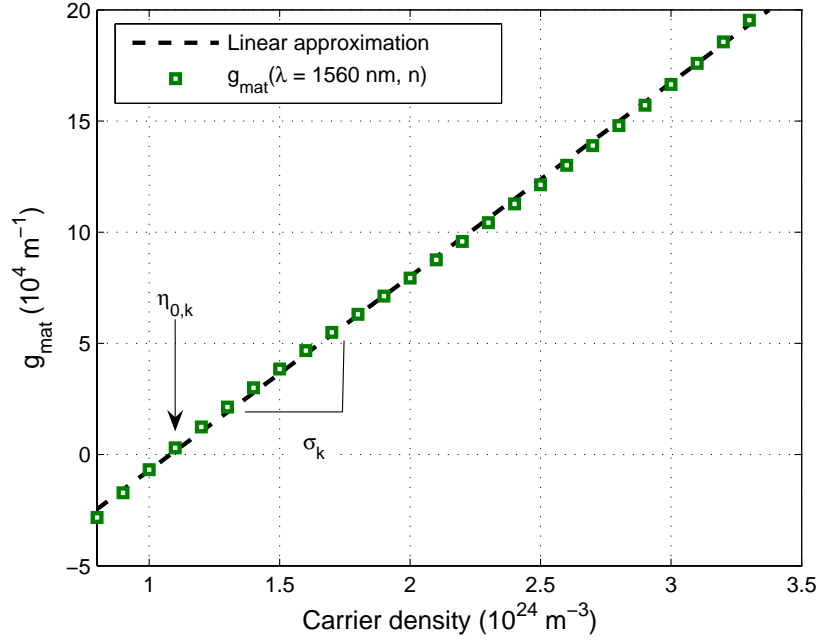


Figure 3. Linear approximation of the gain coefficient $g_{mat}(\lambda, n)$ at 1560 nm

amplifier, the power of each of the N_{sig} signals and each of the N_{ASE} ASE components is calculated according to the value of the reservoir in slice i as in (14). Since the output of slice i becomes the input of slice $i + 1$, we write

$$\tilde{P}_{i+1}^{in} = \tilde{P}_i^{out} e^{-\alpha_s L/N_z} \quad (20)$$

where the length of each slice is given by L/N_z . This procedure reduces the overall gain of the amplifier independently of the signals wavelengths of the carrier density inside the amplifier. In our simulation, the value $\alpha_s L = 1$ was used. At the input and output facets, an extra coefficient c_{add} was used in addition to the ordinary coupling coefficients c_{in} and c_{out} . As proposed by Obermann,² the effective input power \tilde{P}_{in} (at $z = 0$) and effective output power \tilde{P}_{out} (at $z = L$) are respectively

$$\tilde{P}^{in}(t) = \frac{c_{in}}{c_{add}} P^{in}(t) \quad (21)$$

$$\tilde{P}^{out}(t) = \left[c_{out} c_{add} e^{-\alpha_s L/N_z} \right] P^{out}(t) \quad (22)$$

where the coefficient c_{add} is defined as

$$c_{add} = e^{-0.32\alpha_s L/N_z} . \quad (23)$$

Using this method, it is possible to improve the description of the overall gain obtained with the reservoir model. The difference between this method and the first one presented is its effect in the spectral content of the signal. The lumped losses $e^{-\alpha_s L}$ are the same for every wavelength.

The difference between these two methods can be seen in Figure 4. Operating on the gain with (18) affects the slope and carrier density at transparency in different ways. The slope $\sigma(\lambda)$ of the gain coefficient $g_{mat}(\lambda, n)$ differs from the slope of $g_{res}(\lambda, n)$ by a factor K_1 . However, the difference in the carrier densities at transparency for $g_{mat}(\lambda, n)$ and $g_{res}(\lambda, n)$ changes dramatically with the wavelength. As can be seen in Figure 4, the change from η_0 to n_0 increase the spectral curvature, the variation of the carrier density as a function of the wavelength.

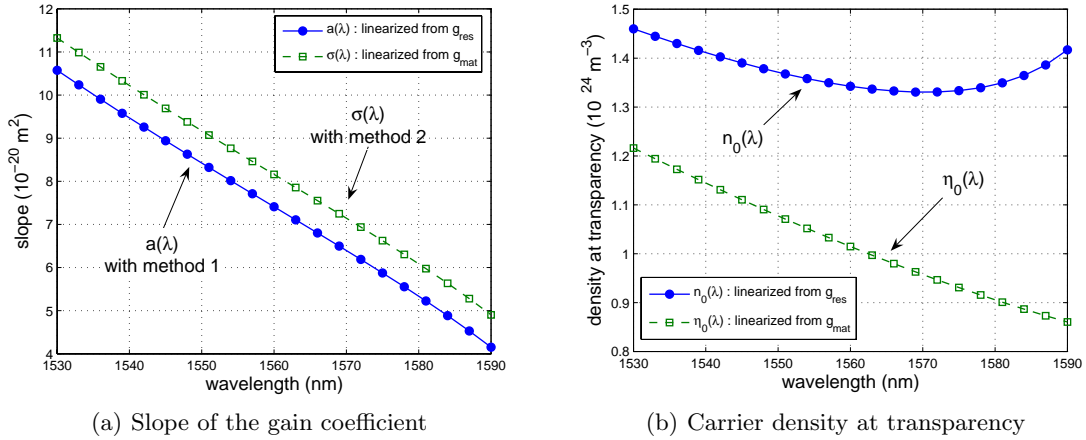


Figure 4. Coefficients of the linear approximation of the gain coefficient. The curves obtained with method 1 using the modified gain coefficient $g_{res}(\lambda, n)$ are represented by circles. The curves obtained with the second method using the original coefficient $g_{mat}(\lambda, n)$ are represented by squares.

5. SIMULATION RESULTS

As discussed in Section 4.3, the gain of the amplifier obtained by using the reservoir model with the gain coefficient $g_{mat}(\lambda, n)$ is overestimated. The previous Section also describes two different methods to obtain a more realistic gain description and a better match between simulation results and experimental data. As we show in this section the spectral content is greatly affected by the choice of the method.

5.1. Gain Saturation

The first figure of merit chosen to compare methods 1 and 2 is the gain saturation $G(\lambda = 1560 \text{ nm}, P_{in})$ at the signal's wavelength. In our case, the fiber-to-fiber gain (including input and output coupling losses) at 1560 nm is unaffected by the choice of the gain coefficient. Both $g_{mat}(\lambda, n)$ and $g_{res}(\lambda, n)$ give good results as shown in Figure 5. By introducing lumped losses (method 2) while being able to vary the α_s factor allows us to obtain a good match with experimental data.

5.2. Gain Spectrum

The second figure of merit used to compare both method 1 from Section 4.3.1 and method 2 from section 4.3.2 is the overall gain spectrum $G(\lambda)$. On the one hand, the overall gain spectrum obtained by using the reservoir model with the transformed gain coefficient $g_{res}(\lambda, n)$ (method 1) is correctly positioned and shows a good agreement with experimental data. On the other hand, the gain spectrum obtained using the lumped losses (method 2) is shifted toward the longer wavelengths, as shown in Figure 5.

5.3. Pulse

The third figure of merit adopted to compare methods 1 and 2 is the shape of an amplified optical pulse. As was demonstrated in Section 5.1, the gain spectrum obtained using method 2 is shifted in wavelength. However, a shifted gain spectrum also has the adverse effect of overestimating the ASE power at the output of the SOA. From Figure 5 we see that the gain spectrum is much larger than the experimental values for wavelengths longer than 1560 nm, where there is no signal. The ASE generated at these wavelengths is too powerful (in simulations) and saturates the SOA, making it difficult to adequately model the dynamic regime.

Figure 6 shows the pulses obtained using methods 1 and 2. The pulse obtained with the lumped losses method shows a constant offset from the experimental data. The offset is due to the extra ASE generated in the SOA. The inset of Figure 6 shows the level of ASE generated by the SOA. The upper curve in the inset is the ASE power obtained with the lumped loss method while the lower curve is the ASE power obtained with the transformation of the gain given by (18).

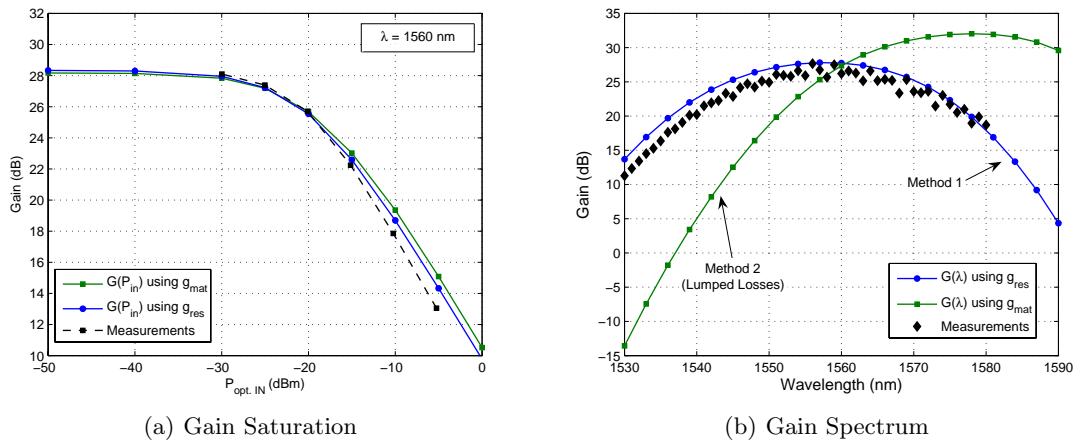


Figure 5. Gain saturation and gain spectrum obtained with the reservoir model using two different methods to reintroduce scattering losses. The results were obtained using the reservoir algorithm with 5 slices.

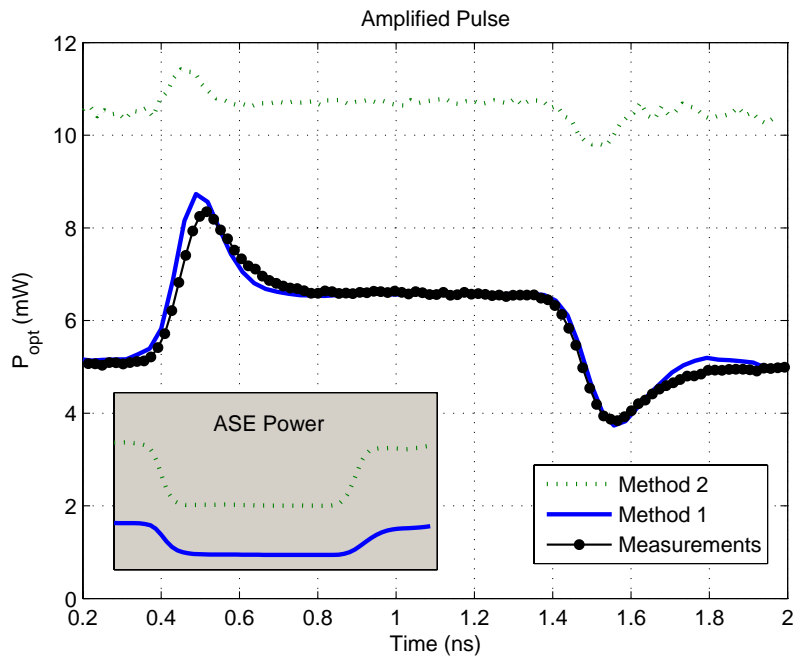


Figure 6. Amplified optical pulse obtained using both techniques of Sections 4.3.1 and 4.3.2. The inset shows the temporal evolution of the ASE power at the output of the SOA during the amplification of the pulse (same scale as the main figure).

6. CONCLUSION

A fast and efficient state-variable model called the reservoir model was discussed and compared with a more complete space-resolved model. To develop the reservoir model, an important term representing the scattering losses was dropped, and we show that adequate modeling cannot be achieved without it. We examine the gain and discuss two methods to adapt it in order to respect the fundamental hypotheses of the reservoir model. The first method slightly transforms the gain by subtracting the scattering losses directly from the gain coefficient while the second method uses the gain coefficient as it is, but introduces lumped losses along the amplifier's

length. We show that the first method gives a good prediction of the gain spectrum, but that the second does not. The transformation proposed in the first method allow the use of the fast reservoir model and still obtain satisfactory results.

ACKNOWLEDGMENTS

This work was supported in part by FQRNT (PADCO FT076892), Canadian Institute for Photonic Innovation (grant CG082485), and by the Italian Ministry project WONDER.

REFERENCES

1. T. Durhuus, B. Mikkelsen, C. Joergensen, S. L. Danielsen, and K. E. Stubkjaer, "All-optical wavelength conversion by semiconductor optical amplifiers," *IEEE J. Lightwave Technol.* **14**, pp. 942–954, 1996.
2. K. Obermann, S. Kindt, D. Breuer, and K. Petermann, "Performance analysis of wavelength converters based on cross-gain modulation in semiconductor-optical amplifiers," *IEEE J. Lightwave Technol.* **16**, pp. 78–85, 1998.
3. F. Ohman, S. Bishoff, B. Tromborg, and J. M. rk, "Noise and regeneration in semiconductor waveguides with saturable gain and absorption," *IEEE J. Quantum Electron.* **40**, pp. 245–255, 2004.
4. M. Menif, W. Mathlouthi, P. Lemieux, L. A. Rusch, and M. Roy, "Error-free transmission for incoherent broadband optical communications systems using incoherent-to-coherent wavelength conversion," *IEEE J. Lightwave Technol.* **23**, pp. 287–294, 2005.
5. N. K. Das, Y. Yamayoshi, and H. Kawaguchi, "Noise and regeneration in semiconductor waveguides with saturable gain and absorption," *IEEE J. Quantum Electron.* **40**, pp. 245–255, 2004.
6. M. J. Connelly, "Wideband semiconductor optical amplifier steady-state numerical model," *IEEE J. Quantum Electron.* **37**, pp. 439–447, 2001.
7. A. A. Saleh and I. M. I. Habbab, "Effects of semiconductor optical amplifier nonlinearity on the performance of high-speed intensity modulation lightwave systems," *IEEE Trans. Commun.* **38**, pp. 839–846, 1990.
8. W. Mathlouthi, P. Lemieux, M. Salsi, A. Vannucci, A. Bononi, and L. A. Rusch, "Fast and efficient dynamic WDM semiconductor optical amplifier model," *Submitted to IEEE J. Lightwave Technol.* , 2006.
9. G. P. Agrawal and N. A. Olsson, "Self-phase modulation and spectral broadening of optical pulses in semiconductor laser amplifiers," *IEEE J. Quantum Electron.* **25**, pp. 2297–2305, 1989.
10. D. Derickson, *Fiber Optic Test and Measurement*, Prentice Hall, second ed., 1998.
11. M. Salsi, A. Vannucci, A. Bononi, W. Mathlouthi, P. Lemieux, and L. A. Rusch, "A reservoir dynamic model for linear optical amplifiers," *Submitted to ECOC* , 2006.